Surface & Coatings Technology 397 (2020) 125949

Contents lists available at ScienceDirect

Surface & Coatings Technology

journal homepage: www.elsevier.com/locate/surfcoat

Effects of the pack Al content on the microstructure and hot corrosion behavior of aluminide coatings applied on Inconel-600

Sina Mahini, Shahin Khameneh Asl*, Taher Rabizadeh, Hossein Aghajani

Department of Materials Engineering, Faculty of Mechanical Engineering, University of Tabriz, 51666-16471 Tabriz, Iran

ARTICLE INFO

Keywords:
Inconel-600
Pack cementation
Aluminide coatings
Hot corrosion
Scanning electron microscopy
X-ray diffraction

ABSTRACT

In this study, aluminide coatings were successfully synthesized on the nickel-based Inconel-600 superalloy substrates using the pack cementation method. The coatings were produced from the packs containing different amounts of Al in the range of 10 wt% - 30 wt%. For the hot corrosion experiments, the specimens were coated with a thin layer of solid Na_2SO_4 and subsequently placed in a muffle furnace in static air at 900 °C for 96 h.

The surface morphology, the elemental composition and the phase composition of the produced coatings before and after the hot corrosion experiments were characterized using different analytical techniques such as SEM, OM, EDS, and XRD.

The results indicate that increasing the amount of Al in the packs from 10 wt% to 30 wt% decreased the thickness of the as-formed aluminide coatings from 210.8 ± 2 μm to 170.7 ± 3 μm. The produced coatings were also composed of three distinct layers including an outer layer, an inner layer, and a narrow inter-diffusion zone (IDZ). Additionally, the coatings consisted of NiAl and Ni_2Al_3 as major phases and $Al_{86}Cr_{14}$ and $Al_{13}Fe_4$ as minor phases. During the hot corrosion experiments, an Al_2O_3 surface scale was developed on the coatings, which resulted in the protection of the substrates. With 10 wt% Al, the Al_2O_3 surface scale was porous and defective whilst this surface scale peeled off when the Al content in the packs increased to 30 wt%. The best hot corrosion resistance was observed in the presence of 20 wt% Al.

1. Introduction

Due to superior mechanical strength and creep resistance, nickel-based superalloys have been widely used as high-temperature engineering components such as turbine blades [1–4]. However, in different industries, combustion gases create aggressive environments, which cause severe weight loss and degradation of physical properties in these materials [5,6].

Hot corrosion is an accelerated oxidation process that occurs in the presence of sulfate and/or chloride ions [7–9]. It is, therefore, desirable to improve the hot corrosion resistance of nickel-based superalloys. There are various methods to increase the hot corrosion resistance of superalloys among which applying a protective coating is the most efficient one [2,10]. Although different types of coatings such as plasma spraying [11,12] and chemical vapor deposition [13] have recently been utilized, pack cementation is the simplest and the most economical one [14–17].

Pack cementation is a self-generated chemical vapor deposition process carried out in a semi-closed thermodynamic system containing metallic powders (e.g., Al, B_4C, Cr, Si), halide activators (e.g., NH_4Cl, KBF_4, MgF_2) and inert fillers (e.g., $A1_2O_3$, SiC, Si_3N_4) [18–21]. This method is commonly used to apply oxidation and corrosion-resistant coatings not only on superalloys [22–24] but also on plain steels [25], alloy steels [25,26], ferritic-martensitic steels [27], Nb-Si-B alloys [28], graphite [29], low carbon steels [30,31], Ti alloys [32], etc.

Aluminizing [33], boronizing [34,35], chromizing [36], and siliconizing [35,37] are four types of pack cementation process among which the first method is extensively used to produce the hot corrosion-resistant coatings [20].

Many research groups have so far investigated the effects of the pack cementation coating parameters (e.g., the activator content, deposition temperature, etc.) on the physical properties of the aluminide coatings such as thickness and oxidation resistance [22,25,26], but a fundamental understanding of how aluminide coatings form on a substrate is slowly emerging. In literature, it was observed that the oxidation resistance of the aluminide coating produced with spherical Al_2O_3 was higher than that of formed with facet Al_2O_3 [25]. It is also noteworthy that the need for improving the performance of aluminide coatings has led to a modification of these coatings with other elements such as Si, Pt, Cr, Hf, Co, and Ge [23,38–41]. The presence of Co, for

* Corresponding author.
E-mail address: khameneh@tabrizu.ac.ir (S. Khameneh Asl).

https://doi.org/10.1016/j.surfcoat.2020.125949
Received 9 March 2020; Received in revised form 10 May 2020; Accepted 19 May 2020
Available online 23 May 2020

example, increased the corrosion resistance of aluminide coatings due to the co-deposition of Co and Al [23].

A number of studies have also been carried out to explore the effects of Al content on the properties of the coatings produced by using various techniques. Huang et al. [42], for example, studied the oxidation behavior of TiAlN coatings reactive-sputtered from TiAl target alloys with different Al contents of 0, 10, 25, 50, and 60 at.%. Their results indicated that the oxidation resistance of the produced coatings improved with increasing the Al content in the target alloys. In addition, Chwa et al. [43] prepared three types of spray dried powders containing different Al contents (TiO_2, TiO_2–10 wt% Al, TiO_2–20 wt% Al). They observed that the weight percentage of Al influenced the microstructure and the mechanical properties of the nanostructured plasma sprayed TiO_2–Al composite coatings. Furthermore, Tong et al. [22] investigated the low-temperature formation of aluminide coatings on the Ni-based superalloy substrates using the pack cementation process. They indicated that varying the pack Al content between 5 wt% and 30 wt% affected the coating thickness, but neither the microstructure nor the phase distribution of the coatings.

The hot corrosion resistance of an aluminide coating is due to the formation of an adhesive, slow-growing, and protective Al_2O_3 layer in an oxidizing atmosphere [44]. However, it has been reported that the aluminide coatings are not fully protective against the hot corrosion environments such as when exposed to the molten Na_2SO_4 salt [20]. Smialek observed that during the hot corrosion of aluminide coatings, elemental sulfur segregated at grain boundaries, which weakened the oxide-metal interface, and eventually caused spallation [45]. However, the role of the formed Al_2O_3 layer in tackling hot corrosion phenomenon is still debatable. Despite extensive research on improving the quality of the pack cemented aluminide coatings, the effects of pack Al content as the main deposition source on the hot corrosion behavior of the aluminide coatings have not yet been investigated. Moreover, the question of how Al content affects the microstructure of the produced coatings is still open.

In the present study, the effects of pack Al content on the microstructure, elemental composition, phase composition, and hot corrosion resistance of aluminide coatings applied on nickel-based superalloy substrates were investigated. Different analytical techniques such as XRD, SEM, and EDS were utilized to answer the research questions. It was observed that the amount of Al in the packs extensively affects the microstructural and the hot corrosion properties of the produced aluminide coatings and there is an optimal weight percentage of Al at which an aluminide coating with proper hot corrosion resistance was formed.

2. Experimental

2.1. Preparation of aluminide coatings

An Inconel-600 (called hereafter IN-600) sheet, with the chemical composition presented in Table 1, was cut to approximate dimensions of 15 mm × 15 mm × 1 mm and used as nickel-based superalloy substrates. Before applying coatings, the substrates were ground using silicon carbide emery paper up to 1500 grit and cleaned ultrasonically in a 50 vol% acetone/50 vol% ethanol bath for 5 min. Afterward, the substrates were rinsed with distilled water and then dried with a hot air gun at 37 °C.

Table 1
Chemical composition of the tested IN-600 substrates.

IN-600	Element (wt%)								
	Ni	Cr	Fe	Mn	Si	C	Cu	P	S
	74.11	15.88	9.37	0.28	0.21	0.046	0.026	0.015	0.002

Table 2
The chemical composition of the pack powders used to deposit aluminide coatings on the IN-600 substrates.

Coating name	Pack composition (wt%)
Coating 1	10 Al – 10 Ni – 78.5 Al_2O_3 – 1.5 NH_4Cl
Coating 2	20 Al – 10 Ni – 68.5 Al_2O_3 – 1.5 NH_4Cl
Coating 3	30 Al – 10 Ni – 58.5 Al_2O_3 – 1.5 NH_4Cl

To apply aluminide coatings, Al (< 5 μm particle size, 99.5%; Sigma Aldrich) and Ni (< 1 μm particle size, 99.8%; Sigma Aldrich) powders as the main coating materials, Al_2O_3 (< 5 μm particle size, 99.5%; Alfa Aesar) powder as an inert filler, and NH_4Cl (ACS reagent, ≥99.5%; Sigma Aldrich) powder as an activator were fully mixed in a mortar for 60 min. According to the pack compositions tabulated in Table 2, three different packs with various Al contents of 10 wt%, 20 wt%, and 30 wt % were prepared, and the deposited aluminide coatings were called as coating 1, coating 2, and coating 3, respectively. To synthesize the coatings, 30 g of the powder mixture was poured into the Al_2O_3 crucibles and the prepared IN-600 substrates were embedded within the center of each pack. The filled crucibles were closed with a tight-fitting Al_2O_3 lid, sealed with Kaolin paste, and placed in the hot zone of a tube furnace.

The pack cementation process was carried out in a tube furnace at 900 °C for 4 h with the heating rate of 10 °C·min^{-1}, under continuous Ar flow. The inert gas pressure inside the furnace was also adjusted to about 1 atm. Firstly, to remove humidity, the prepared packs were heated from room temperature to 210 °C within 20 min followed by maintaining at this temperature for 30 min under Ar gas flow. Subsequently, the packs were heated up to 900 °C and kept at this temperature for 4 h. Finally, to avoid any oxidation the packs were cooled down inside the furnace to room temperature naturally by cutting off the power supply under flowing Ar. The specimens were then removed from the packs and ultrasonically cleaned.

2.2. Hot corrosion experiments

The hot corrosion resistance of the uncoated and coated specimens was evaluated in a muffle furnace in static air at 900 °C. Before this, the samples were placed on a hot plate and heated up to 200 °C and then uniformly brushed with a supersaturated Na_2SO_4 solution. It is worth noting that the specimens were weighed before and after applying the thin Na_2SO_4 layer to ensure that the amount of salt brushed all over the samples was about 3–4 mg/cm^2. Afterward, the samples were placed in Al_2O_3 crucibles and loaded into the furnace. At regular intervals of 8 h, the specimens were taken out of the furnace, cooled down to room temperature. Then, to remove the remaining unreacted salt, the coupons were immersed and washed in boiling distilled water and dried in air. To measure the weight changes, the samples were weighed with a high-precision analytical balance with an accuracy of 0.01 mg. The hot corrosion experiments were continued by brushing a fresh Na_2SO_4 layer over the specimens. These procedures were repeated several times so that the total hot corrosion time of 96 h was reached.

2.3. Characterization of the coatings

Different analytical techniques were utilized to characterize the formed aluminide coatings before and after the hot corrosion experiments. Optical microscopy (OM; OLYMPUS CK40M-AN) and scanning electron microscopy (SEM; PHENOM ProX) techniques were employed to characterize the surface and the cross-sectional morphology of the specimens. Energy dispersive X-ray spectroscopy (EDS) was used to determine the elemental composition variations on top surface layers and across the specimens. It is also noteworthy that prior to these analyses, the specimens were mounted in resin, carefully ground with

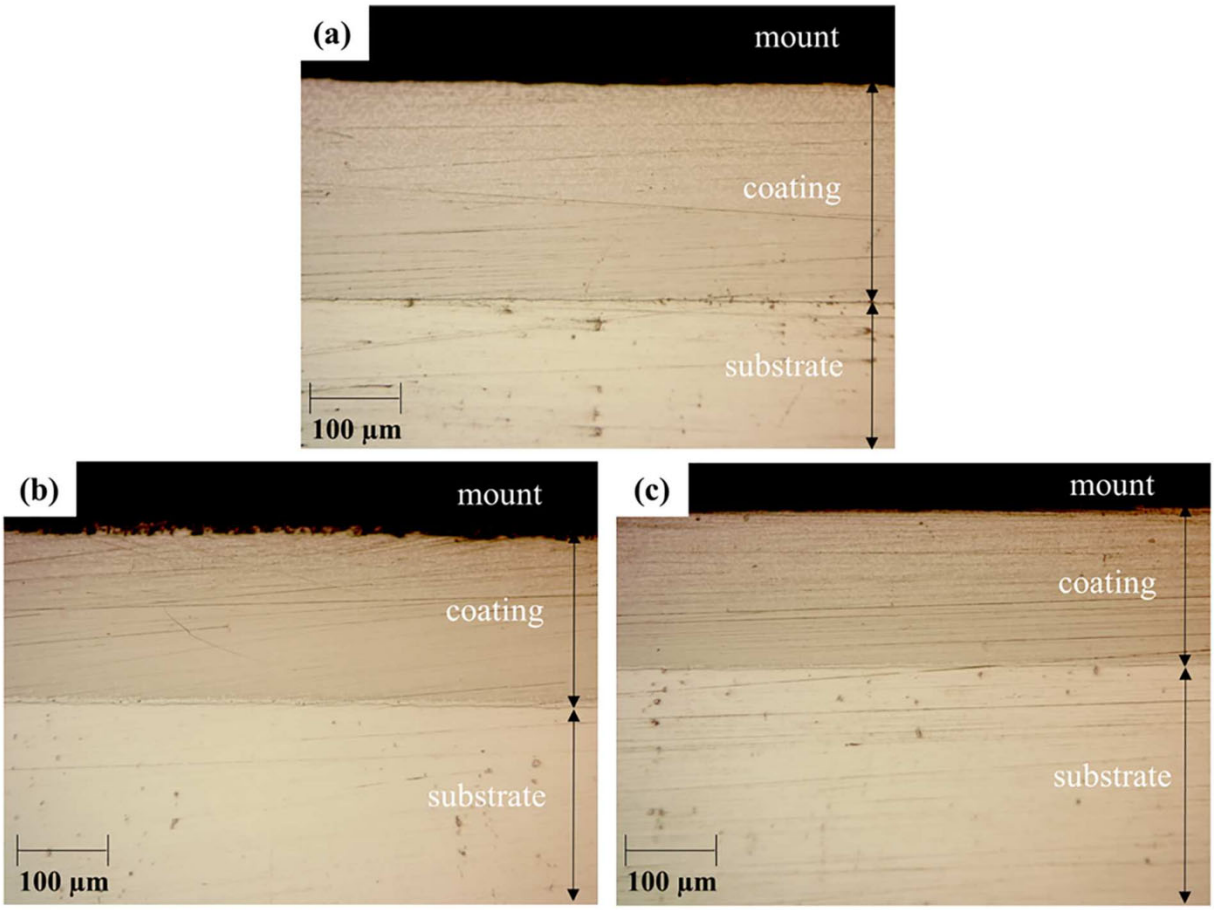

Fig. 1. Optical microscopy images from the cross-section of (a) coating 1 (10 wt% Al); (b) coating 2 (20 wt% Al); (c) coating 3 (30 wt% Al).

SiC emery papers up to 3000 grit followed by polishing with 1 µm diamond slurry, and degreasing in a 50 vol% acetone/50 vol% ethanol bath for 5 min. ImageJ software was also used for any thickness measurements [46]. The phase composition of the specimens was also identified using X-ray diffraction technique (XRD; BRUKER Advance-D8 X-ray diffractometer; 2θ range 20–70°; resolution 0.105°/step; counting time 1 s/step) using Cu K_α (λ = 1.5406 Å) radiation.

3. Results and discussion

3.1. Characterization of the produced coatings

The cross-sectional morphology and the thickness of the as-formed aluminide coatings evaluated using OM are presented in Fig. 1. It can be seen that the pack-cementation aluminide coatings formed on IN-600 were quite uniform without any structural defects (e.g., cracks, voids, and/or inclusions). Moreover, the thickness of coatings 1, 2, and 3 was about 210.8 ± 2 µm, 198.1 ± 2.5 µm, and 170.7 ± 3 µm, respectively.

Fig. 2 illustrates the phase composition of the as-formed coatings. According to the XRD patterns, the precipitated aluminide coatings were composed of some intermetallic phases among which NiAl and Ni_2Al_3 were considered as major phases. These phases formed due to the diffusion of Al from the top surface layers and the diffusion of Ni from the substrate [47,48].

Similarly, other researchers observed NiAl and/or Ni_2Al_3 phases as the major phases in the microstructure of the precipitated aluminide coatings [49,50].

During a successful pack cementation aluminizing process, some sequential reactions take place. At first step, upon heating, $NH_4Cl_{(s)}$ decomposes and produces $NH_{3(g)}$ and $HCl_{(g)}$ (see Reaction (1)). Afterward, at high temperatures of about 400 °C, Al powder reacts with NH_4Cl salts to form gaseous Al-chloride species (e.g., $AlCl_{(g)}$, $AlCl_{2(g)}$, and $AlCl_{3(g)}$) (see Reaction (2)) [19].

$$NH_4Cl_{(s)} \rightleftharpoons NH_{3(g)} + HCl_{(g)} \quad (1)$$

$$2Al_{(s)} + 2HCl_{(g)} \rightleftharpoons 2AlCl_{(g)} + H_{2(g)} \quad (2)$$

Moreover, there is always a gap between the reactants in the pack and the embedded substrate surface, which is called the “aluminum depleted zone”. This zone is formed due to the transport of aluminum into the coating because of the partial pressure gradients between the pack and the coating surface [19]. To form an aluminide layer, gaseous Al-chloride species diffuse to the surface of the substrate via the aluminum-depleted zone and release some active Al atoms (denoted as [Al] in Reaction (3)) [51]. In addition, there is an inverse relationship between the diffusion coefficients of the gaseous Al-chloride species and their molecular weight. Thus, the diffusion of $AlCl_{(g)}$ mainly causes the [Al] formation and its transport to the surface of the substrate (see Reaction (3)):

$$3AlCl_{(g)} \rightleftharpoons 2[Al] + AlCl_{3(g)} \quad (3)$$

Subsequently, [Al] diffuses into the substrate to form an aluminide layer whilst $AlCl_{3(g)}$ moves back to the “undepleted pack” zone and reacts again with Al powder ($Al_{(s)}$) in the pack to reproduce $AlCl_{(g)}$ [19].

The diffusion of [Al] into the substrate (in this research: superalloy IN-600) produces NiAl and Ni_2Al_3. In general, the synthesis of a nickel aluminide, Ni_aAl_b phase occurs according to the following exothermic reaction [52,53]:

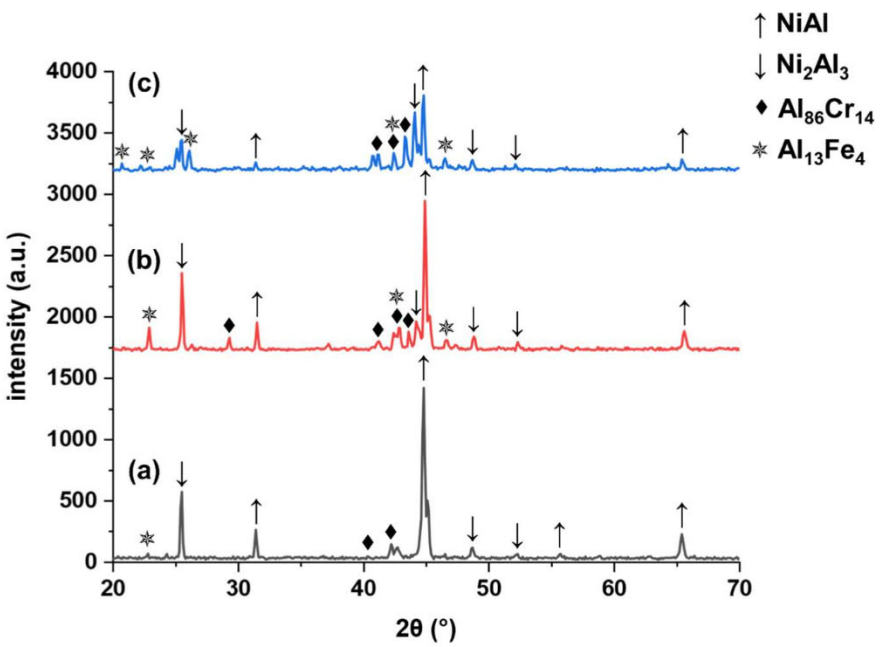

Fig. 2. XRD patterns of the samples with (a) coating 1; (b) coating 2; (c) coating 3.

$$aNi_{(s)} + b[Al] \rightleftharpoons Ni_aAl_{b(s)} + Heat \quad (i.e.\ for\ a = b = 1, Ni_aAl_b = NiAl) \tag{4}$$

Besides NiAl and Ni_2Al_3, there are usually some minor phases (e.g., in this research: $Al_{86}Cr_{14}$ and $Al_{13}Fe_4$) formed due to the diffusion reactions between the active Al atoms produced in the pack and the substrate elements (e.g., Cr, Fe) [54]. $Al_{86}Cr_{14}$ and $Al_{13}Fe_4$ are intermetallic compounds produced by the following reactions:

$$14Cr(s) + 86[Al] \rightleftharpoons Al_{86}Cr_{14(s)} \tag{5}$$

$$4Fe_{(s)} + 13[Al] \rightleftharpoons Al_{13}Fe_{4(s)} \tag{6}$$

It is also obvious from the XRD patterns that by increasing the pack Al content from 10 wt% in coating 1 to 30 wt% in coating 3, the NiAl peak intensities decreased indicating a considerable reduction in the amount of this major phase (Fig. 2). Moreover, the number of $Al_{86}Cr_{14}$ and $Al_{13}Fe_4$ peaks increased, which was due to the further diffusion of Al into the substrate.

The surface morphology of the produced coatings was further evaluated using SEM and EDS analyses. The results demonstrated the multi-phase and multi-elemental composition of the surface layers of the synthesized coatings. As an example, it can be seen that the surface of coating 2 was not uniform and two different regions in color (i.e., grey and black) were identified (Fig. 3(a), (b)). As demonstrated by EDS analysis, the black regions were rich in Al whilst the greyish spots were rich in Ni (Fig. 3(d)). Moreover, the secondary electron SEM images from the surface of the aluminide coatings demonstrate that the formed aluminide coating had a bedded structure (see Fig. 3(c) for coating 2).

EDS was also utilized to measure the surface elemental composition (in at.%) of the deposited coatings (Fig. 4). As can be seen, Al and Ni were the two main elements on the surface of the coatings indicating the formation of NiAl and Ni_2Al_3 phases during the pack cementation process. Moreover, increasing the pack Al level from 10 wt% in coating 1 to 30 wt% in coating 3, raised the amount of Al on the surface of the coatings from 73.4 ± 2.1 at.% to 75.5 ± 3.8 at.% whilst the atomic percent of Ni on the surface of the coatings decreased slightly from 22.3 ± 1.4 at.% to 18.3 ± 1.9 at.%. Furthermore, the at.% of Cr and Fe increased slightly from 2.5 ± 1.3 at.% to 3.8 ± 0.8 at.% and 1.8 ± 1.1 at.% to 2.4 ± 0.6 at.%, respectively, which was related to the enhanced diffusion of Al into the substrate when the Al level increased three times from pack 1 to pack 3.

Besides optical microscopy, the cross-section of the aluminide coatings was characterized in detail using SEM and EDS. As an example, it is clear from Fig. 5(a) that coating 2 was composed of three distinct layers including an outer layer, an inner layer, and a narrow inter-diffusion zone (IDZ). The outer layer (see Fig. 5(b)) was not homogeneous and plenty of black precipitates were dispersed across this layer. According to the EDS analysis (Fig. 5(c)), the black precipitates were composed of an Al-rich phase containing other elements such as Ni, Cr, and Fe [23]. In contrast, the greyish regions were rich in Ni. According to the XRD patterns and the EDS analysis (see Figs. 2 and 5(c)), the black (spot 1) and the greyish (spot 2) areas were mainly the light phase Ni_2Al_3, and the heavy phase NiAl, respectively.

In contrast, the inner layer was quite uniform and a negligible amount of black precipitates were observed indicating the presence of NiAl in this area. It is also clear from Fig. 5(a) that a high amount of Ni_2Al_3 black precipitates were present near the surface and their concentration decreased gradually by moving towards the inner layer and diminished at the coating/substrate interface. Zhou et al. [54] and Tong et al. [22] reported similar microstructure but Qiao et al. [23] and He et al. [24] only observed an outer layer containing some Al_2O_3 precipitates and a diffusion zone at the coating/substrate interface.

These results illustrate the reason for the observed decrease in the thickness of the as-formed aluminide coatings when the amount of Al in the packs increased from 10 wt% to 30 wt% (see Fig. 1). In general, nickel aluminide diffusion coatings are formed via either primarily singular inward Al diffusion or predominantly singular outward Ni diffusion [47,55,56]. It has been reported that a low process temperature (e.g. below 1000 °C) and high Al activity in the pack lead to the inward Al diffusion, which mainly forms the Ni_2Al_3 intermetallic phase in the coating. On the other hand, a high process temperature (e.g. 1100 °C or higher) with low Al activity in the pack results in the outward Ni diffusion, which forms NiAl [57].

Therefore, it can be said that the aluminide coatings in this study were deposited basically through the inward diffusion of Al. However, according to Fig. 5(a), the presence of a narrow IDZ beneath the coating inner layer suggests that a limited degree of outward Ni diffusion occurred [47,58,59]. Furthermore, the thick outer layer containing mainly Ni_2Al_3 and some NiAl suggests the considerable inward Al diffusion, whilst the thin inner layer of NiAl indicates the occurrence of limited outward diffusion of Ni (see Fig. 5(a)).

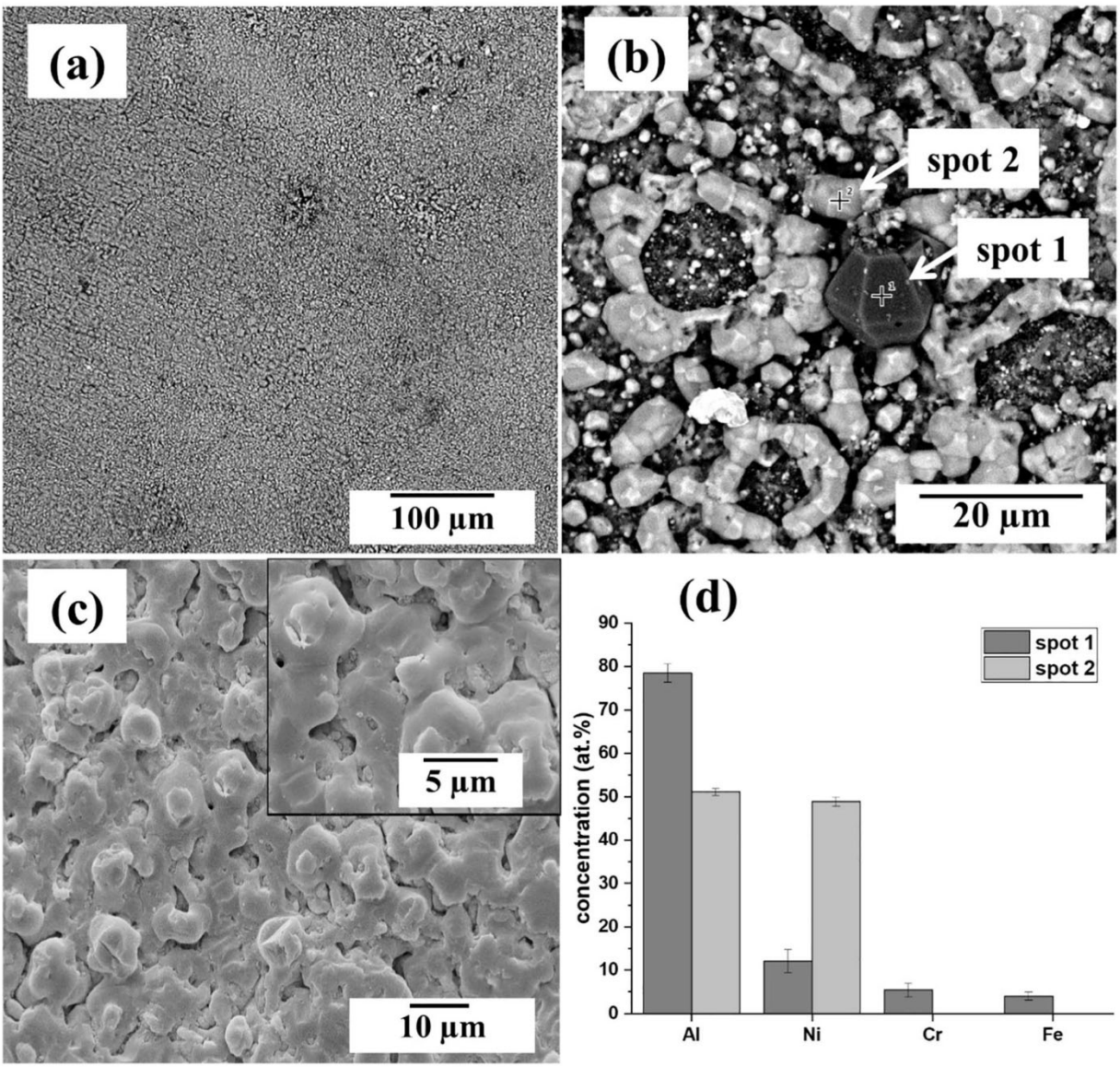

Fig. 3. Surface analysis of coating 2 (a) low magnification BSE analysis; (b) high magnification BSE analysis; (c) high magnification SE analysis; (d) EDS analysis of spots 1 and 2.

In addition, increasing the pack Al content from 10 wt% in coating 1 to 30 wt% in coating 3, enhanced the activity of Al. As a result, the intensity of inward Al diffusion increased, which led to the effective reaction of Al with the other substrate elements (e.g., Cr and Fe) and thus the formation of a higher number of Al−Cr and Al−Fe intermetallic precipitates in the coating outer layer (see the XRD peaks of $Al_{86}Cr_{14}$ and $Al_{13}Fe_4$ detected for coating 3 in Fig. 2). On the other hand, increasing the Al activity limited the outward diffusion of Ni, which in turn resulted in a lower content of the major phase NiAl (see the XRD peaks of NiAl detected for coating 3 in Fig. 2).

The elemental depth profiles of the produced coatings are shown in Fig. 6. For instance, it is obvious that by moving from the surface of coating 2 towards the substrate, the atomic percent of Ni increased from 20.3 ± 2.6 at.% to 69.3 ± 2.1 at.% (Fig. 6(b)). Meanwhile, the amount of Al decreased slightly from 73.8 ± 3.5 at.% in the surface layer to 41.1 ± 2.4 at.% in the inter-diffusion zone but dropped sharply to 5.6 ± 1.8 at.% in the substrate.

Furthermore, the concentration of Cr in the substrate was 16.2 ± 1.4 at.%, but after an increase to 19 ± 2.2 at.% in the IDZ layer, the corresponding value dropped to 8.6 ± 2.7 at.% in the inner layer. An increase in the Cr concentration in the IDZ layer was because of the low solubility of this element in Al [60], which resulted in a very low diffusion rate of this element in the inner and outer layers of the synthesized aluminide coating. Therefore, the accumulation of Cr at the coating/substrate interface and the formation of a Cr-rich phase were detected [20]. According to Datta and Xiang studies [58], the outward diffusion of the substrate elements such as Ni, Cr, Fe, and Co is fully compensated by the inward diffusion flow of Al, and thus no Kirkendall voids are formed in the IDZ area.

Moreover, the concentration of Fe dropped continuously form 8.9 ± 1.7 at.% in the substrate to 2.1 ± 1.2 at.% in the coating surface. Similar trends in the elemental concentration profiles were observed for coatings 1 and 3 (see Fig. 6(a), (c)).

3.2. Hot corrosion tests

The XRD patterns of the uncoated IN-600 and the samples with coatings 1, 2, and 3, which were exposed to Na_2SO_4 salt at 900 °C for 96 h, are presented in Fig. 7. It can be seen that after hot corrosion experiments Cr_2O_3 was formed on the bare substrate (Fig. 7(a)). Besides

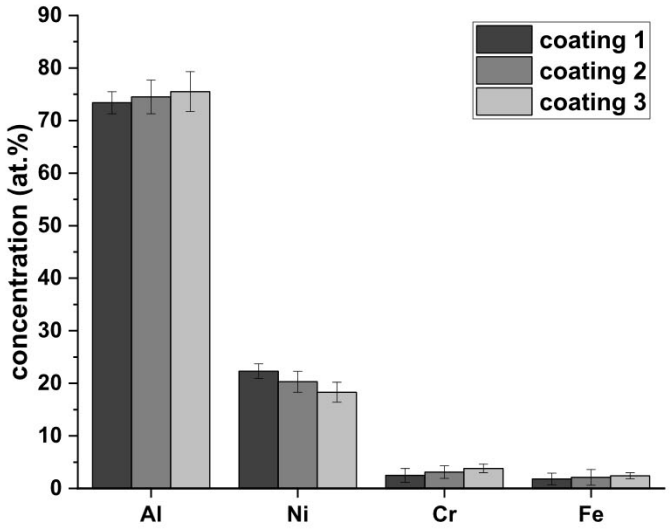

Fig. 4. Average elemental composition measured from the surface of coatings 1, 2, and 3.

Cr_2O_3, Fe_2O_3 and $FeNi_3$ were detected on IN-600 demonstrating the severe corrosion of the substrate due to the lack of protection against the diffusion of destructive oxygen and sulfur ions. This is in agreement with the findings reported by Bennett et al. [61] and Bai et al. [20].

In comparison to IN-600, an Al_2O_3 scale was formed on the surface of coatings 1, 2, and 3. The formation of this oxide layer originated from the interaction of Al with oxygen and was accompanied by the consumption of Al in the aluminide layer of the as-formed coatings. This oxide scale also acted as a diffusion barrier against the diffusion of oxygen and sulfur ions.

Furthermore, it is obvious that the minor phases $Al_{13}Fe_4$ and $Al_{86}Cr_{14}$ observed in the XRD spectrums of the as-formed aluminide coatings, had disappeared indicating the consumption of Al on the way of producing Al_2O_3 scale during the hot corrosion process (Fig. 7 vs. Fig. 2). Moreover, NiAl was still detected in the XRD spectra of the hot corroded aluminized specimens (e.g., a sharp peak at $2\theta = 44.5°$) further confirming the proper hot corrosion protection of the produced aluminide coatings.

Fig. 8 illustrates the changes in the weight of the uncoated and coated IN-600 samples during the hot corrosion process due to the formation, spallation, and/or dissolution of the formed surface oxide

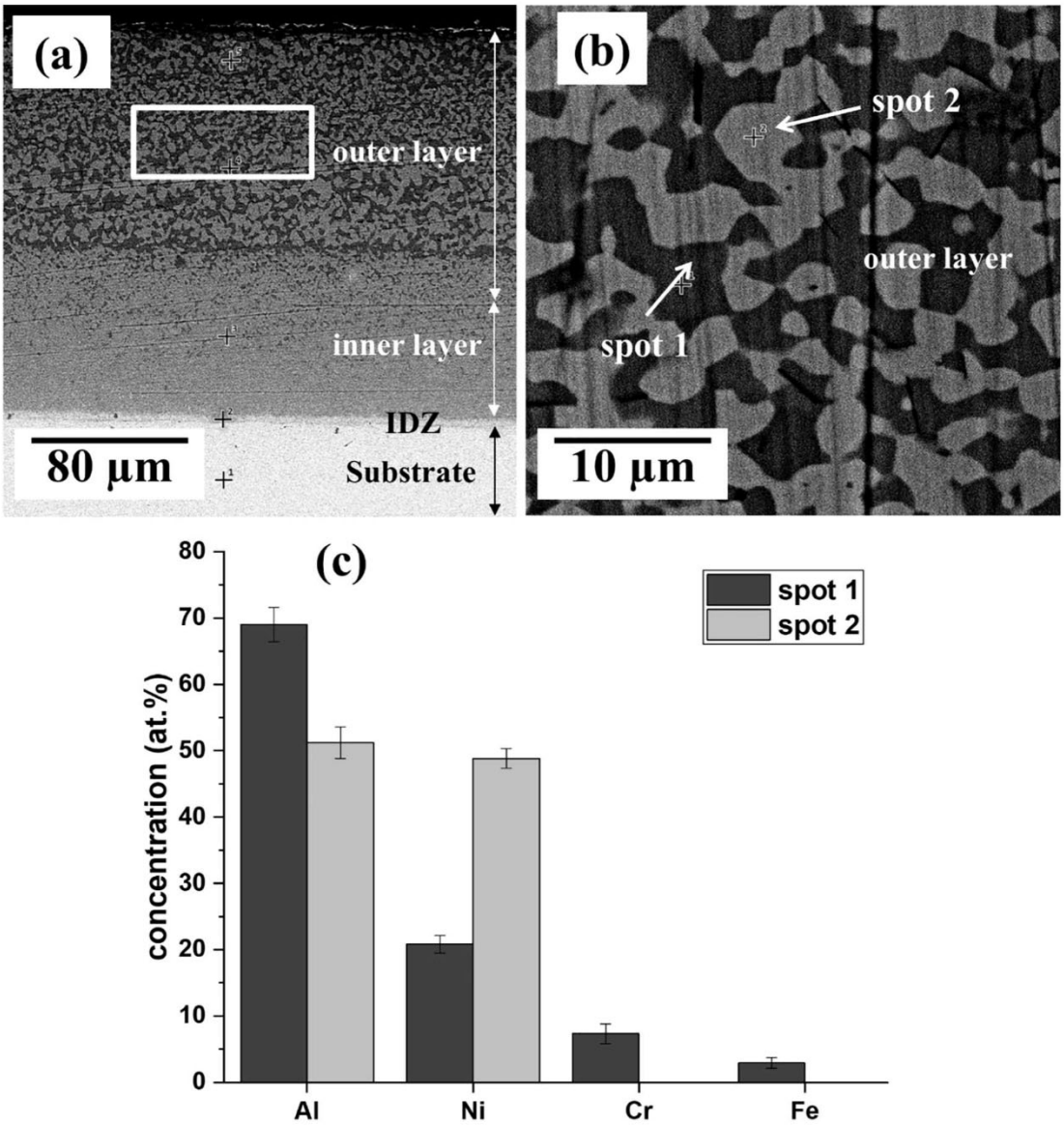

Fig. 5. SEM image of coating 2 (a) cross-sectional image; (b) outer layer; and (c) EDS analysis of the outer layer.

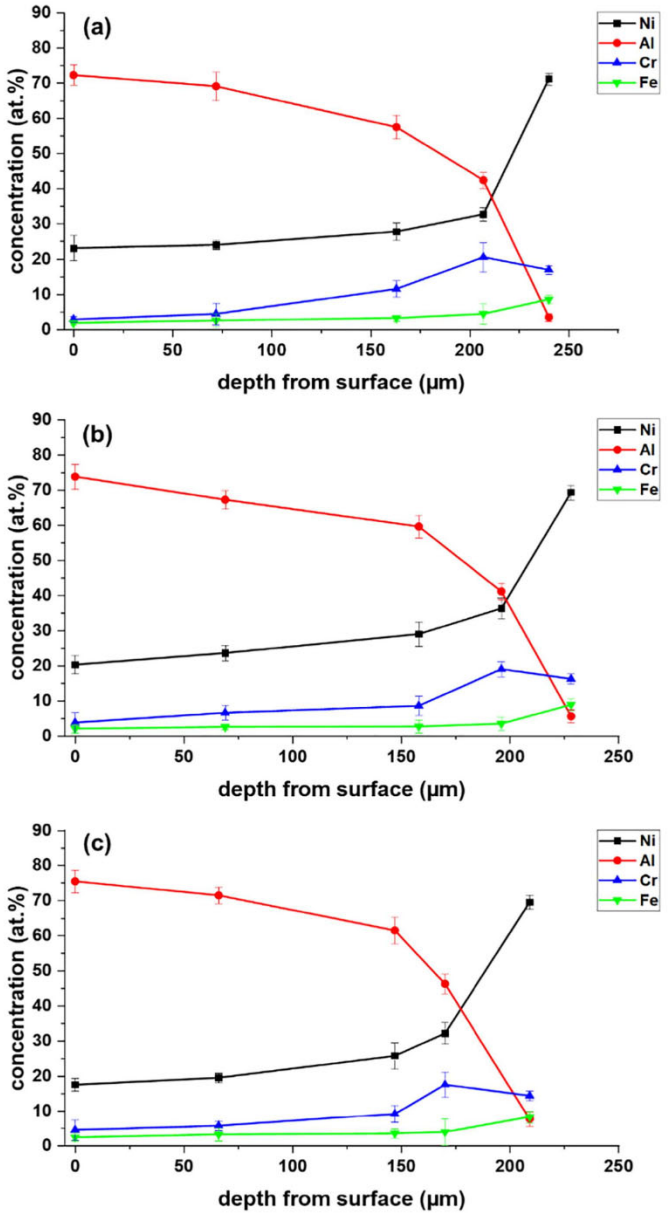

Fig. 6. The elemental depth profile related to (a) coating 1; (b) coating 2; (c) coating 3.

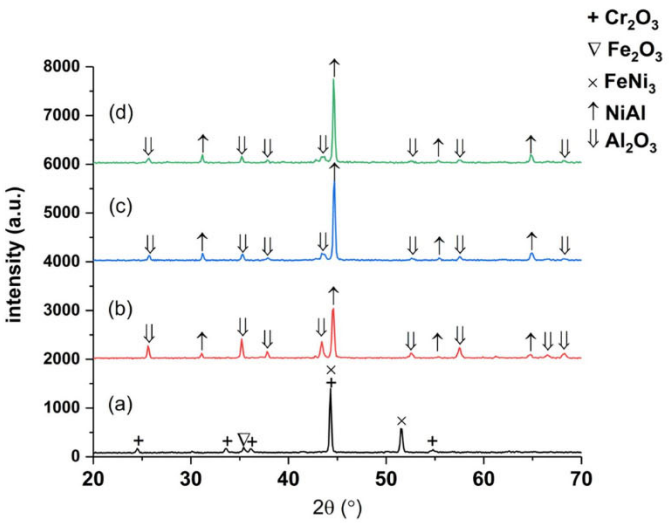

Fig. 7. XRD spectrums of (a) the uncoated IN-600, and the samples with (b) coating 1; (c) coating 2; (d) coating 3, after the hot corrosion test in Na_2SO_4 salt at 900 °C for 96 h.

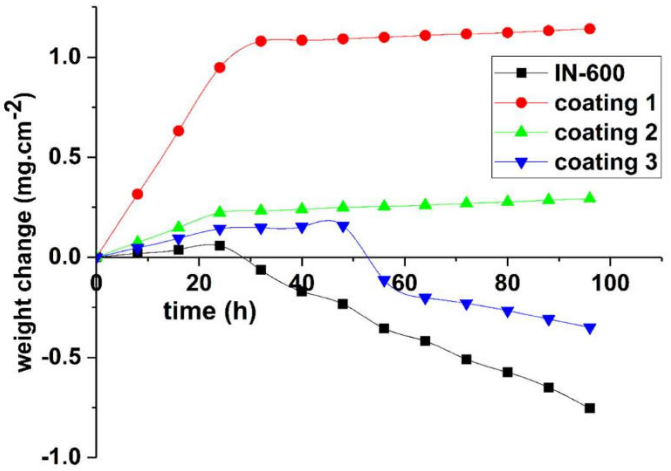

Fig. 8. Hot corrosion kinetic curves for the uncoated IN-600 and the samples with coatings 1, 2, and 3.

scales.

For the uncoated IN-600, during the first 24 h, a weight gain of 0.058 mg/cm^2 was measured, which was related to the formation of Cr_2O_3 surface scale. This scale was not stable and partially transformed into volatile CrO_3, which evaporated at 900 °C [62,63]. Thus, the presence of a discontinuous and non-protective Cr_2O_3 layer resulted in the diffusion of oxygen and sulfur ions into the inner layers and the gradual dissolution of the substrate in the presence of molten Na_2SO_4 salt. As a result, a severe weight loss of 0.755 mg/cm^2 was measured between 24 h and 96 h of the corresponding hot corrosion experiment.

For the sample with coating 1, during the first 24 h, a noticeable weight gain of 0.948 mg/cm^2 was observed, which was related to the formation of an Al_2O_3 surface scale. After 24 h, the rate of weight gain decreased and after 32 h the corresponding curve leveled off. Therefore, the total weight gain of about 1.142 mg/cm^2 was recorded after 96 h.

The hot corrosion kinetic curve of the sample with coating 2 had a similar trend to that of the sample with coating 1. However, during the first 24 h, this specimen gained about four times less weight than that of the sample with coating 1 (0.223 mg/cm^2 vs. 0.948 mg/cm^2). This indicates the formation of a thinner Al_2O_3 surface scale on the sample with coating 2, thus it limited oxygen diffusion better than coating 1. As a result, coating 2 was probably more compact than coating 1. Moreover, after 24 h, the corresponding hot corrosion kinetic curve reached a plateau and the total weight gain of about 0.293 mg/cm^2 was recorded after 96 h.

In contrast, the hot corrosion kinetic curve of the sample with coating 3 had a different development trend comparing to the other two curves plotted for the samples with coatings 1 and 2. During the first 24 h, the weight gain for this sample was less than that of the sample with coating 2 (0.143 mg/cm^2 vs. 0.223 mg/cm^2). Similar to the mechanism suggested above, coating 3 was possibly more compact than coating 2. However, beyond 48 h, the Al_2O_3 scale formed on the coating 3 peeled off, which caused the exposure of the substrate and/or the aluminide layer to the corrosive environment and thus considerable weight loss of 0.350 mg/cm^2 was recorded after 96 h. Here, it is noteworthy that the observed spallation was probably due to the presence of the high content of minor phases in the outer layer of the corresponding coating. Hence, the differences in the thermal expansion coefficient between the minor phases and the major phases led to the failure of the coating.

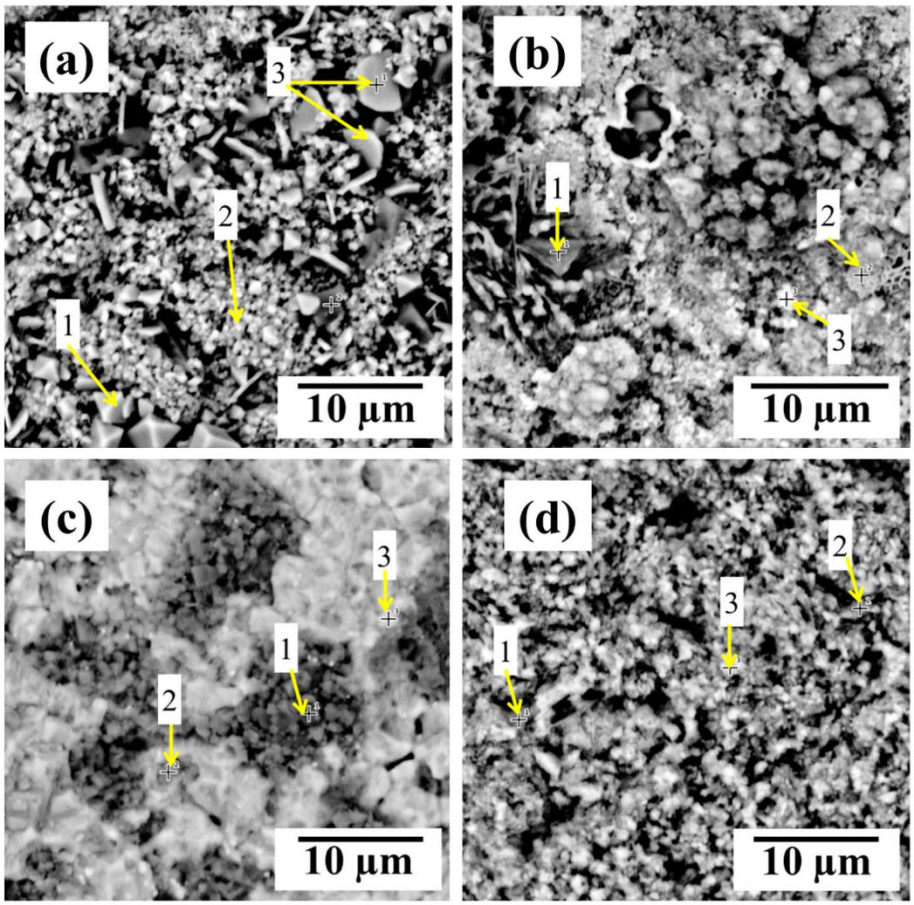

Fig. 9. SEM surface image of (a) the uncoated IN-600, and the samples with (b) coating 1; (c) coating 2; (d) coating 3, after the hot corrosion test in Na_2SO_4 salt at 900 °C for 96 h.

Table 3
The surface EDS analysis of the specimens after the hot corrosion test.

Specimen	Spot	Element (at.%)				
		Al	O	Ni	Fe	Cr
Uncoated IN-600	1	–	68.5	2.5	3.6	25.3
	2	–	69.2	2.4	1.1	27.2
	3	–	61.3	3.9	0.6	34.1
Sample with coating 1	1	33.3	65.4	1.2	–	–
	2	37.9	45.5	16.6	–	–
	3	32.7	45.7	21.6	–	–
Sample with coating 2	1	40.7	57.2	2.1	–	–
	2	33.3	63.1	3.6	–	–
	3	41.7	41.7	16.6	–	–
Sample with coating 3	1	44	54.5	1.5	–	–
	2	29.7	64.6	5.6	–	–
	3	39.6	25.4	35	–	–

The surface morphology and the elemental composition of the uncoated and coated specimens exposed to Na_2SO_4 salt at 900 °C for 96 h were studied using SEM and EDS analyses (Fig. 9 and Table 3). According to Fig. 9(a), the hot corrosion products formed on the bare substrate had almost pyramidal (spot 1), fine grain (spot 2), and blade-like (spot 3) morphologies. As indicated in Table 3, Cr and O were the main elements present on the surface of the hot corroded IN-600, which together with a little amount of Fe demonstrate the formation of Cr_2O_3 and Fe_2O_3 phases on the bare IN-600 specimen. As reported by Nguyen et al. [64] and Zou et al. [65], the fine grain and blade morphologies observed in this research were most probably related to the formation of Cr_2O_3, whereas Fe_2O_3 had pyramidal morphology. Additionally, Ni was identified after the hot corrosion experiments of the uncoated substrate (see Table 3), which was probably related to the $FeNi_3$ phase present under the surface Cr_2O_3 scale.

Comparing with the substrate, the hot corroded samples with aluminide coatings had different surface morphologies. As an example, the surface of the sample with coating 2 was covered with a bright layer mainly composed of Al and O demonstrating the formation of an Al_2O_3 surface scale (see Fig. 9(c) and Table 3). The detected Ni was also related to NiAl present under the Al_2O_3 surface scale (see Fig. 7(c)). Moreover, the reason for the observed regions with different colors was related to the thickness of the Al_2O_3 layer. In fact, in dark regions, the thickness of the Al_2O_3 scale was relatively high and a very low amount of Ni (about 2.1 at.%) was measured. However, in bright regions the thickness of the Al_2O_3 layer was relatively low, and a high amount of Ni (about 16.6 at.%) was detected. This was almost true for the surface morphologies observed for the hot corroded samples with coatings 1 and 3 (see Fig. 9(b) and (d)).

The cross-section of the substrate and the coated samples were evaluated after the hot corrosion experiments. Based on Fig. 10(a), during the hot corrosion process, a thin layer was formed on IN-600, which, based on the XRD analysis, was mainly made of Cr_2O_3. The enlarged SEM image of this layer reveals the defective nature of the formed surface oxide scale with an average thickness of 3.9 µm (see Fig. 10(b)).

On the other hand, the Al_2O_3 scale formed on the surface of the sample with coating 1 during the hot corrosion test was porous and defective (Fig. 10(c) and (d)), which was in contrast to the more uniform, denser, and protective Al_2O_3 surface layer observed on the sample with coating 2 (Fig. 10(e) and (f)), and further confirms the better hot

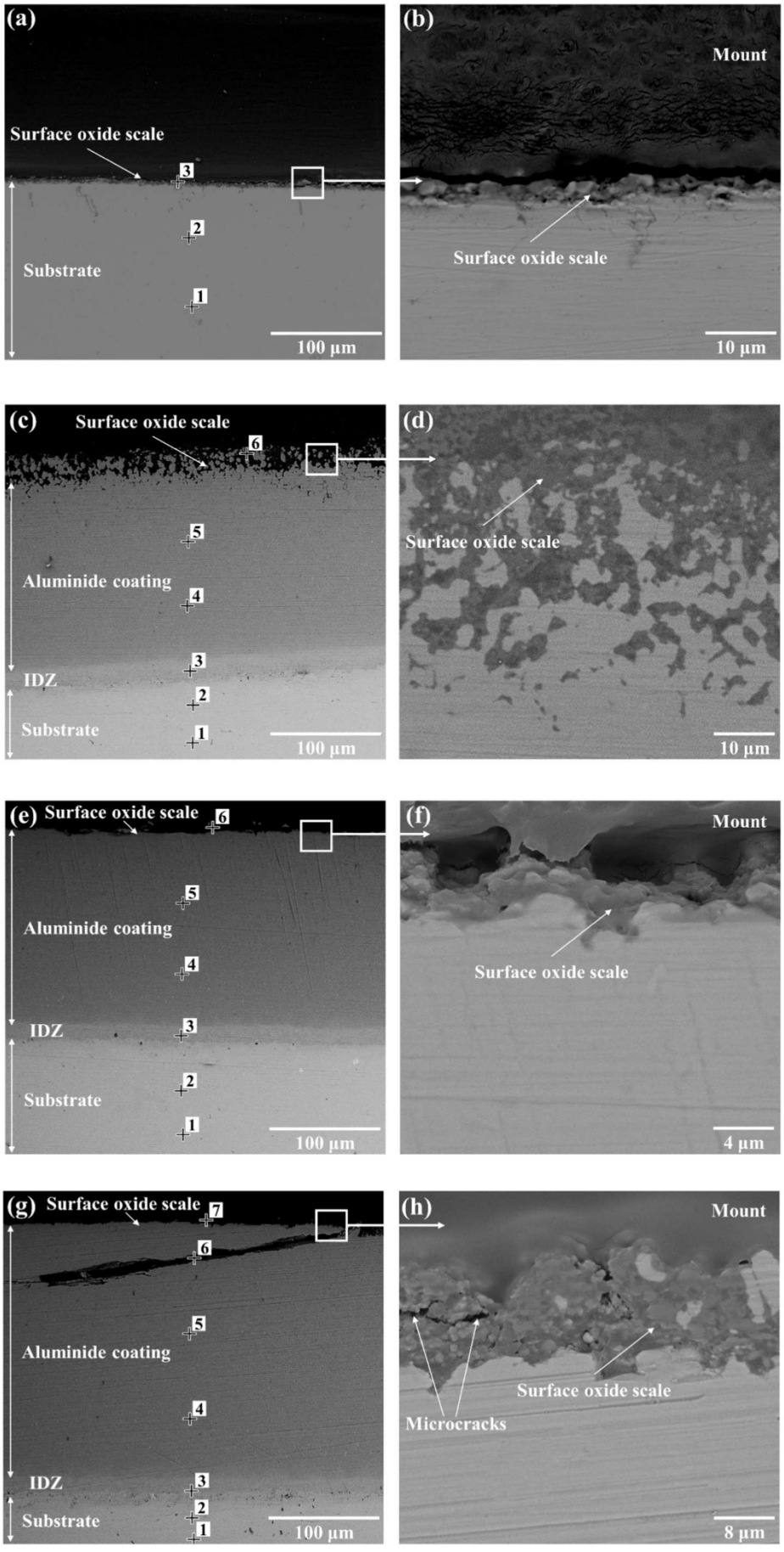

(caption on next page)

Fig. 10. SEM cross-sectional image of (a, b) the uncoated IN-600; (c, d) the sample with coating 1; (e, f) the sample with coating 2; (g, h) the sample with coating 3 after hot corrosion test in Na_2SO_4 salt at 900 °C for 96 h.

corrosion resistance of the sample with coating 2. Additionally, the thickness of the Al_2O_3 surface oxide scale formed on coatings 1 and 2 were about 41.9 and 3.8 μm, respectively (see Fig. 10(d) and (f)).

Unlike the samples with coatings 1 and 2, serious cracks were observed in the oxide scale and outer layer of the sample with coating 3. These defects facilitated the penetration of oxygen and sulfur ions into the coating, and thus led to the internal oxidation and sulfidation of this sample (Fig. 10(g) and (h)). Moreover, the measured thickness of the Al_2O_3 surface scale was about 13.3 μm.

It should also be noted that after the hot corrosion experiments the thickness of coatings 1, 2, and 3 increased about 12.2 μm, 5.4 μm and 92.6 μm, respectively (see Figs. 10 and 1). It is true that the corrosive environment of the molten salt Na_2SO_4 decreases the coating thickness. This is, however, insignificant here due to the presence of the Al_2O_3 surface oxide scale, which acts as a diffusion barrier against molten Na_2SO_4 salts. The observed increase in the thickness of the coatings may result from two mechanisms: (1) during the hot corrosion experiments, the inward diffusion of Al from the coating to the substrate occurred, which resulted in the phase transformation of Ni_2Al_3 to NiAl (see also Fig. 7), hence the black Ni_2Al_3 precipitates disappeared (compare Fig. 5(a) with Fig. 10(e)) and the thickness of the coatings increased [57]. (2) Another probable reason is that during the hot corrosion process, oxygen is absorbed by the microcracks developed on the aluminide coating surface (called high-temperature oxidation), which leads to an increase in the aluminide coating thickness. Based on the second mechanism, by considering the changes in the thickness of the produced coatings, it is deduced that the sample with coating 2 had the best hot corrosion resistance due to the lowest oxygen absorption further confirming the formation of a denser Al_2O_3 surface oxide scale on this sample (Fig. 10(f)). In contrast, the sample with coating 3 had the worst hot corrosion resistance due to the highest oxygen absorption showing the presence of a non-protective and seriously cracked Al_2O_3 surface oxide scale (Fig. 10(h)).

The cross-section of the samples after the hot corrosion tests was further studied using EDS analysis (Table 4). For the uncoated IN-600, just Ni (73 at.%), Cr (17.2 at.%), and Fe (9.8 at.%) were detected in the substrate (spots 1 and 2). This demonstrates that sulfur did not diffuse deeply into the substrate. Moreover, the presence of a high amount of O and Cr in the surface scale (spot 3) indicates the formation of a Cr_2O_3 layer on top of the sample. On the other hand, the presence of Fe (1.4 at.%) in spot 3 reveals the formation of a Fe_2O_3 layer, whilst the detected Ni (3 at.%) was related to the $FeNi_3$ phase present under the surface oxide scale.

Table 4
The cross-sectional EDS analysis of the specimens after the hot corrosion test.

Specimen	Spot	Element (at.%)					
		Al	O	Ni	Fe	Cr	S
Uncoated IN-600	1	–	–	73	9.8	17.2	–
	2	–	–	72.6	9.7	17.7	–
	3	–	68.2	3	1.4	27.3	–
Sample with coating 1	1	4.5	–	71.3	7.9	16.3	–
	2	7.7	–	67.6	8.2	16.5	–
	3	30.8	–	49.9	3.4	15.9	–
	4	53.3	–	37.7	4.5	4.5	–
	5	55.5	–	35.1	3.7	5.7	–
	6	35.9	61.6	2.5	–	–	–
Sample with coating 2	1	3.8	–	71.4	8.4	16.4	–
	2	6.8	–	68.8	7.5	16.9	–
	3	32.9	–	43.4	5.7	18	–
	4	55.1	–	36.7	3.7	4.5	–
	5	55.8	–	26.7	3.6	13.9	–
	6	40.4	54.6	5	–	–	–
Sample with coating 3	1	6.1	–	68.2	8.5	17.2	–
	2	8.2	–	61.2	8.7	21.9	–
	3	10.4	–	20	5.9	63.7	–
	4	51.4	–	40.3	4	4.3	–
	5	52.3	–	34.7	3.7	9.2	–
	6	28.9	24.5	33.3	–	5.1	8.1
	7	32.9	45.1	22	–	–	–

Considering the samples with coatings 1 and 2, the amount of Ni decreased continuously from 71.3 at.% and 71.4 at.% in the substrate (spot 1) to 35.1 at.% and 26.7 at.% in the outer layer of the coatings (spot 5), respectively. Whereas, the amount of Al increased continuously from 4.5 at.% and 3.8 at.% in the substrate (spot 1) to 55.5 at.% and 55.8 at.% in the outer layer of the coatings (spot 5), respectively, further illustrating the outward diffusion of Ni and the inward diffusion of Al. Besides, Al and O were mainly detected in spot 6 indicating the formation of an Al_2O_3 scale on top of the coatings 1 and 2. Moreover, elemental sulfur was neither detected in spots 1 and 2 (in the substrate) nor in spots 3, 4, and 5 (in the coating), representing the proper protective effects of the formed Al_2O_3 scale during the hot corrosion process.

Unlike the samples with coatings 1 and 2, the amount of Ni and Al changed irregularly across the hot corroded sample with coating 3 (see Table 4). This issue was probably due to the presence of cracks in the coating, which resulted in the internal oxidation and sulfidation (see Table 4). Moreover, the amount of Ni in spot 7 was more than Al and O, confirming the spallation of the Al_2O_3 surface oxide scale.

It should be mentioned that during the hot corrosion process, the Na_2SO_4 layer present on the surface of the coatings is melted, and reacts with the formed protective Al_2O_3 scale (see Reactions (7) and (8)) [66]:

$$Na_2SO_4 \rightleftharpoons Na_2O + SO_2 + 1/2O_2 \quad (7)$$

$$Al_2O_3 + Na_2O \rightleftharpoons 2AlO_2^- + 2Na^+ \quad (8)$$

Then, because of the concentration gradient at the salt/Al_2O_3 scale and at the salt/air interfaces, the produced AlO_2^- migrates from the salt/Al_2O_3 scale interface to the salt/air interface where the alkalinity of the molten salt is low and thus, Al_2O_3 re-precipitates via the decomposition of AlO_2^- species (see Reaction (9)) [24]:

$$2AlO_2^- \rightleftharpoons Al_2O_3 + O^{2-} \quad (9)$$

The released O^{2-} raises the alkalinity of the salt/Al_2O_3 scale interface and thus, accelerates the fluxing of the Al_2O_3 scale according to Reaction (8). This self-cycling process consumes more and more Al from the inner layers of the aluminide coating. However, the re-precipitated Al_2O_3 will be more porous and more fragile than the former Al_2O_3 scale [24]. According to Fig. 8, during the first 24 h of the hot corrosion tests, the sample with coating 1 experienced significant weight gain than the other two samples (compare the slope of the weigh change vs. time curves). This indicates that the Al_2O_3 layer formed on the sample with coating 1 was thicker and fast-growing. As a result of the high growth rate, a high content of defects was produced across the Al_2O_3 scale. These microstructural defects allowed the penetration of the molten Na_2SO_4 salt and, thus the mechanism suggested above led to the formation of a porous Al_2O_3 layer on the sample with coating 1 (Reactions (7)–(9); Fig. 10(c) and (d)). However, this issue did not occur for the samples with coatings 2 and 3 (Fig. 10(f) and (h)), which was due to the formation of thinner, denser, and slow-growing Al_2O_3 layer (see also Fig. 8).

Considering the hot corrosion results, among the produced coatings, coating 1 was the least compact one, which did not thoroughly limit the oxygen diffusion. As a result, this coating produced the thickest, fast-growing, and highly porous Al_2O_3 scale. In addition, this coating had a low content of minor phases in its outer layer, which made the

spallation very unlikely to occur. Hence, it demonstrated acceptable hot corrosion resistance. On the other hand, the coating 3 was the most compact coating which significantly limited the diffusion of oxygen. Therefore, the thinnest, slowest-growing, and densest Al_2O_3 layer was formed on top of this coating during the initial stages of the corrosion test. However, beyond 48 h, this Al_2O_3 scale peeled off which was due to a high content of minor phases across the outer layer of this coating. Therefore, coating 3 exhibited the worst hot corrosion resistance. Finally, the compactness and minor phases content of coating 2 was between the other two coatings. In other words, this coating was compact enough to effectively limit the oxygen diffusion and thus to provide a thin and dense Al_2O_3 scale. In addition, it consisted of a moderate content of minor phases so as to avoid the spallation of the Al_2O_3 layer. Therefore, the addition of 20 wt% Al in the pack, resulted in an optimal hot corrosion resistant aluminide coating.

4. Conclusions

Aluminide coatings were applied on nickel-based Inconel-600 substrates using the pack cementation method. The coatings had three different regions called “outer layer”, “inner layer” and “inter-diffusion zone (IDZ)”. The results indicate that the aluminide coatings were formed due to the predominant inward Al diffusion along with a limited degree of outward Ni diffusion. These two mutual diffusion processes lead to the formation of NiAl and Ni_2Al_3 as major phases and $Al_{86}Cr_{14}$ and $Al_{13}Fe_4$ as minor phases.

During the hot corrosion process, an Al_2O_3 layer was formed on the surface of the coatings, which was capable of protecting the aluminized specimens against the diffusion of oxygen and sulfur ions, and reducing the hot corrosion rate to an acceptable extent.

Among the coated specimens, the aluminide coating formed in the presence of 20 wt% Al revealed the least weight changes (0.293 mg/cm^2 after the test) and the lowest hot corrosion rate. Therefore, the hot corrosion resistance of the specimens is summarized as: the sample with coating 2 (20 wt% Al in the pack) > the sample with coating 1 (10 wt % Al in the pack) > the sample with coating 3 (30 wt% Al in the pack) > the uncoated superalloy IN-600 specimen.

CRediT authorship contribution statement

Sina Mahini: Methodology, Data curation, Writing - original draft. **Shahin Khameneh Asl**: Data curation, Supervision. **Taher Rabizadeh**: Data curation, Writing - original draft, Writing - review & editing. **Hossein Aghajani**: Data curation.

Declaration of competing interest

The authors declare that they have no known competing financial interests or personal relationships that could have appeared to influence the work reported in this paper.

References

[1] N.S. Stoloff, C.T. Sims, W.C. Hagel, Superalloys II, Wiley, 1987.
[2] G.W. Goward, Progress in coatings for gas turbine airfoils, Surf. Coatings Technol. 108–109 (1998) 73–79, https://doi.org/10.1016/S0257-8972(98)00667-7.
[3] A.C. Yeh, K.W. Lu, C.M. Kuo, H.Y. Bor, C.N. Wei, Effect of serrated grain boundaries on the creep property of Inconel 718 superalloy, Mater. Sci. Eng. A 530 (2011) 525–529, https://doi.org/10.1016/j.msea.2011.10.014.
[4] T. Trosch, J. Strößner, R. Völkl, U. Glatzel, Microstructure and mechanical properties of selective laser melted Inconel 718 compared to forging and casting, Mater. Lett. 164 (2016) 428–431, https://doi.org/10.1016/j.matlet.2015.10.136.
[5] J.A. Goebel, F.S. Pettit, G.W. Goward, Mechanisms for the hot corrosion of nickel-base alloys, Metall. Trans. 4 (1973) 261–278, https://doi.org/10.1007/BF02649626.
[6] A.K. Gupta, J.P. Immarigeon, P.C. Patnaik, Review of factors controlling the gas turbine hot section environment and their influence on hot salt corrosion test methods, High Temp. Technol. 7 (1989) 173–186, https://doi.org/10.1080/02619180.1989.11753435.
[7] P. Hancock, Vanadic and chloride attack of superalloys., Mater. Sci. Technol. 3 (1986) 536–544. doi:https://doi.org/10.1080/02670836.1987.11782265.
[8] N. Eliaz, G. Shemesh, R.M. Latanision, Hot corrosion in gas turbine components, Eng. Fail. Anal. 9 (2002) 31–43, https://doi.org/10.1016/S1350-6307(00)00035-2.
[9] R.A. Rapp, Hot corrosion of materials: a fluxing mechanism? Corros. Sci. 44 (2002) 209–221, https://doi.org/10.1016/S0010-938X(01)00057-9.
[10] F. Wang, H. Lou, L. Bai, W. Wu, High temperature corrosion 2. R. Streiff, J. Stringer, RC Krutenat, M. Caillet Eds. (Elseveier science Publ., barking, UK, 1989) pp. 387-389, Mat. Sci. Eng. A. 121 (1989) 387–389.
[11] D. Degout, F. Kassabji, P. Fauchais, Titanium dioxide plasma treatment, Plasma Chem. Plasma Process. 4 (1984) 179–198, https://doi.org/10.1007/BF00566840.
[12] J.A. Haynes, E.D. Rigney, M.K. Ferber, W.D. Porter, Oxidation and degradation of a plasma-sprayed thermal barrier coating system, Surf. Coatings Technol. 86–87 (1996) 102–108, https://doi.org/10.1016/S0257-8972(96)02985-4.
[13] J. Müller, M. Schierling, E. Zimmermann, D. Neuschütz, Chemical vapor deposition of smooth α-Al2O3 films on nickel base superalloys as diffusion barriers, Surf. Coatings Technol. (1999) 16–21, https://doi.org/10.1016/S0257-8972(99)00333-3.
[14] H.W. Hsu, W.T. Tsai, High temperature corrosion behavior of siliconized 310 stainless steel, Mater. Chem. Phys. 64 (2000) 147–155, https://doi.org/10.1016/S0254-0584(99)00264-3.
[15] C.H. Koo, T.H. Yu, Pack cementation coatings on Ti3Al-Nb alloys to modify the high-temperature oxidation properties, Surf. Coatings Technol. 126 (2000) 171–180, https://doi.org/10.1016/S0257-8972(00)00546-6.
[16] C. Zhou, H. Xu, S. Gong, Y. Yang, K. Young Kim, A study on aluminide and Cr-modified aluminide coatings on TiAl alloys by pack cementation method, Surf. Coatings Technol. 132 (2000) 117–123, https://doi.org/10.1016/S0257-8972(00)00911-7.
[17] Y. Wang, S. Feng, D. Liu, C. Zhang, J. Xu, C. Luo, J. Suo, Preparation of layered α-Al 2 O 3/TiO 2 composite coating by pack cementation process and subsequent thermochemical treatment, Surf. Coatings Technol. 330 (2017) 277–284, https://doi.org/10.1016/j.surfcoat.2017.10.031.
[18] S.C. Kung, R.A. Rapp, Kinetic study of aluminization of Iron by using the pack cementation technique, J. Electrochem. Soc. 135 (1988) 731–741, https://doi.org/10.1149/1.2095732.
[19] B. Meyers, S. Lynn, ASM Handbook Volume 5: Surface Engineering, ninth ed, ASM International, Materials Park, Ohio, 1994.
[20] C.Y. Bai, Y.J. Luo, C.H. Koo, Improvement of high temperature oxidation and corrosion resistance of superalloy IN-738LC by pack cementation, Surf. Coatings Technol. 183 (2004) 74–88, https://doi.org/10.1016/j.surfcoat.2003.10.011.
[21] T. Murakami, K. Matsuzaki, Y. Gomi, S. Sasaki, H. Inui, Microstructure and tribological properties of gray cast iron specimens coated by aluminizing, boronizing, chromizing and siliconizing, Mater. Res. Soc. Symp. Proc. (2013) 115–120, https://doi.org/10.1557/opl.2012.1726.
[22] L. Tong, Y. Dengzun, Z. Chungen, Low-temperature formation of aluminide coatings on Ni-base superalloys by pack cementation process, Chinese J. Aeronaut. 23 (2010) 381–385, https://doi.org/10.1016/S1000-9361(09)60231-4.
[23] M. Qiao, C. Zhou, Hot corrosion behavior of Co modified NiAl coating on nickel base superalloys, Corros. Sci. 63 (2012) 239–245, https://doi.org/10.1016/j.corsci.2012.06.027.
[24] H. He, Z. Liu, W. Wang, C. Zhou, Microstructure and hot corrosion behavior of Co-Si modified aluminide coating on nickel based superalloys, Corros. Sci. 100 (2015) 466–473, https://doi.org/10.1016/j.corsci.2015.08.011.
[25] K. Mohammadi, A.K. Haghi, A study on characterization of pack-cemented aluminide coating on metals, J. Mater. Process. Technol. 201 (2008) 669–672, https://doi.org/10.1016/j.jmatprotec.2007.11.273.
[26] Z.D. Xiang, P.K. Datta, Relationship between pack chemistry and aluminide coating formation for low-temperature aluminisation of alloy steels, Acta Mater. 54 (2006) 4453–4463, https://doi.org/10.1016/j.actamat.2006.05.032.
[27] D. Fähsing, C. Oskay, T.M. Meißner, M.C. Galetz, Corrosion testing of diffusion-coated steel in molten salt for concentrated solar power tower systems, Surf. Coatings Technol. 354 (2018) 46–55, https://doi.org/10.1016/j.surfcoat.2018.08.097.
[28] J. Cheng, S. Yi, J.S. Park, Simultaneous coating of Si and B on Nb-Si-B alloys by a halide activated pack cementation method and oxidation behaviors of the alloys with coatings at 1100 °C, J. Alloys Compd. 644 (2015) 975–981, https://doi.org/10.1016/j.jallcom.2015.05.003.
[29] J. Pourasad, N. Ehsani, In-situ synthesis of SiC-ZrB2coating by a novel pack cementation technique to protect graphite against oxidation, J. Alloys Compd. 690 (2017) 692–698, https://doi.org/10.1016/j.jallcom.2016.08.112.
[30] G. Vourlias, N. Pistofidis, D. Chaliampalias, E. Pavlidou, G. Stergioudis, E.K. Polychroniadis, D. Tsipas, Zinc deposition with pack cementation on low carbon steel substrates, J. Alloys Compd. 416 (2006) 125–130, https://doi.org/10.1016/j.jallcom.2005.08.037.
[31] Q. Xue, C. yuan Sun, J.Y. Yu, L. Huang, J. Wei, J. Zhang, Microstructure evolution of a Zn-Al coating co-deposited on low-carbon steel by pack cementation, J. Alloys Compd. 699 (2017) 1012–1021, https://doi.org/10.1016/j.jallcom.2016.12.291.
[32] Y.G. Zhao, W. Zhou, Q.D. Qin, Y.H. Liang, Q.C. Jiang, Effect of pre-oxidation on the properties of aluminide coating layers formed on Ti alloys, J. Alloys Compd. 391 (2005) 136–140, https://doi.org/10.1016/j.jallcom.2004.07.073.
[33] Y. Sun, J. Dong, P. Zhao, B. Dou, Formation and phase transformation of aluminide coating prepared by low-temperature aluminizing process, Surf. Coatings Technol. 330 (2017) 234–240, https://doi.org/10.1016/j.surfcoat.2017.10.025.
[34] K.G. Anthymidis, N. Maragoudakis, G. Stergioudis, O. Haidar, D.N. Tsipas, A comparative study of boride coatings obtained by pack cementation method and by fluidized bed technology, Mater. Lett. 57 (2003) 2399–2403, https://doi.org/10.

1016/S0167-577X(02)01243-0.
[35] R. Swadźba, High temperature oxidation behavior of C103 alloy with boronized and siliconized coatings during 1000 h at 1100 °C in air, Surf. Coatings Technol. 370 (2019) 331–339, https://doi.org/10.1016/j.surfcoat.2019.04.019.
[36] Y.B. Zhou, H. Chen, H. Zhang, Y. Wang, Preparation and oxidation of an Y2O3-dispersed chromizing coating by pack cementation at 800 °C, Vacuum 82 (2008) 748–753, https://doi.org/10.1016/j.vacuum.2007.10.010.
[37] M. Mitoraj-Królikowska, E. Godlewska, Silicide coatings on Ti-6Al-1Mn (at.%) alloy and their oxidation resistance, Surf. Coatings Technol. 334 (2018) 491–499, https://doi.org/10.1016/j.surfcoat.2017.12.004.
[38] J.A. Haynes, B.A. Pint, K.L. More, Y. Zhang, I.G. Wright, Influence of sulfur, platinum, and hafnium on the oxidation behavior of CVD NiAl bond coatings, Oxid. Met. 58 (2002) 513–544, https://doi.org/10.1023/A:1020525123056.
[39] P. Volovitch, J.E. Masse, A. Fabre, L. Barrallier, W. Saikaly, Microstructure and corrosion resistance of magnesium alloy ZE41 with laser surface cladding by Al-Si powder, Surf. Coatings Technol. 202 (2008) 4901–4914, https://doi.org/10.1016/j.surfcoat.2008.04.052.
[40] S.A. Azarmehr, K. Shirvani, A. Solimani, M. Schütze, M.C. Galetz, Effects of Pt and Si on the low temperature hot corrosion of aluminide coatings exposed to Na 2 SO 4-60 Mol% V 2 O 5 salt, Surf. Coatings Technol. 362 (2019) 252–261, https://doi.org/10.1016/j.surfcoat.2019.01.116.
[41] M.C. Galetz, C. Oskay, S. Madloch, Microstructural degradation and interdiffusion behavior of NiAl and Ge-modified NiAl coatings deposited on alloy 602 CA, Surf. Coatings Technol. 364 (2019) 211–217, https://doi.org/10.1016/j.surfcoat.2019.02.048.
[42] J.-L. Huang, B.-Y. Shew, Effects of aluminum concentration on the oxidation behaviors of reactively sputtered TiAlN films, J. Am. Ceram. Soc. 82 (2004) 696–704, https://doi.org/10.1111/j.1151-2916.1999.tb01819.x.
[43] S.O. Chwa, D. Klein, F.L. Toma, G. Bertrand, H. Liao, C. Coddet, A. Ohmori, Microstructure and mechanical properties of plasma sprayed nanostructured TiO2-Al composite coatings, Surf. Coatings Technol. 194 (2005) 215–224, https://doi.org/10.1016/j.surfcoat.2004.07.080.
[44] J. Ma, S.M. Jiang, H.Q. Li, W.X. Wang, J. Gong, C. Sun, Microstructure and oxidation behaviour of an AlSiY/NiCrAlYSi composite coating at 1150°C, Corros. Sci. 53 (2011) 1417–1423, https://doi.org/10.1016/j.corsci.2011.01.004.
[45] J.L. Smialek, Adherent Al2O3 scales formed on undoped NiCrAl alloys, (1987).
[46] C.T. Rueden, J. Schindelin, M.C. Hiner, B.E. DeZonia, A.E. Walter, E.T. Arena, K.W. Eliceiri, Image J2: ImageJ for the next generation of scientific image data, BMC Bioinformatics 18 (2017), https://doi.org/10.1186/s12859-017-1934-z.
[47] G.W. Goward, D.H. Boone, Mechanisms of formation of diffusion aluminide coatings on nickel-base superalloys, Oxid. Met. 3 (1971) 475–495, https://doi.org/10.1007/BF00604047.
[48] O.K. Das, V. Singh, S.V. Joshi, Evolution of aluminide coating microstructure on nickel-base cast superalloy CM-247 in a single-step high-activity aluminizing process, Metall. Mater. Trans. A Phys. Metall. Mater. Sci. 29 (1998) 2173–2188, https://doi.org/10.1007/s11661-998-0042-0.
[49] H. Arabi, S. Rastgari, Z. Salehpour, A. Bakhshi, Formation mechanism of silicon modified aluminide coating on a Ni-base superalloy, http://194.225.230.88/files/mateng/arabi_88fcd/formation_mechanism_of_silicon_modified.pdf, (2008) , Accessed date: 20 December 2019.
[50] H.-X. Wang, Y. Zhang, J.-L. Cheng, Y.-S. Li, High temperature oxidation resistance and microstructure change of aluminized coating on copper substrate, Trans. Nonferrous Met. Soc. China. 25 (2015) 184–190, https://doi.org/10.1016/S1003-6326(15)63594-4.
[51] C. Fu, W.K. Kong, G.H. Cao, Microstructure and oxidation behavior of Al + Si co-deposited coatings on nickel-based superalloys, Surf. Coatings Technol. 258 (2014) 347–352, https://doi.org/10.1016/j.surfcoat.2014.09.003.
[52] K. Morsi, Review: reaction synthesis processing of Ni-Al intermetallic materials, Mater. Sci. Eng. A 299 (2001) 1–15, https://doi.org/10.1016/S0921-5093(00)01407-6.
[53] C. Fu, C.H. Wang, Z.M. Ren, G.H. Cao, Comparison of microstructure and oxidation behavior between Pt-free and Pt-modified δ-Ni2Si coatings on Ni-based superalloys, Corros. Sci. 98 (2015) 211–222, https://doi.org/10.1016/j.corsci.2015.05.030.
[54] F. Zhou, M. Gao, G.F. Tu, K. Liu, K.W. Pengu, Aluminide coating prepared on Ni-base superalloy by pack cementation, Adv. Mater. Res. (2014) 11–17, https://doi.org/10.4028/www.scientific.net/AMR.848.11.
[55] Z.D. Xiang, P.K. Datta, Codeposition of Al and Si on nickel base superalloys by pack cementation process, Mater. Sci. Eng. A 356 (2003) 136–144.
[56] R. Mévrel, C. Duret, R. Pichoir, Pack cementation processes, Mater. Sci. Technol. (United Kingdom). 2 (1986) 201–206, https://doi.org/10.1179/mst.1986.2.3.201.
[57] P. C. Patnaik, Intermetallic coatings for high temperature applications—a review, Mater. Manuf. Process. 4 (1989) 133–152, https://doi.org/10.1080/10426918908956276.
[58] Z.D. Xiang, J.S. Burnell-Gray, P.K. Datta, Aluminide coating formation on nickel-base superalloys by pack cementation process, J. Mater. Sci. 36 (2001) 5673–5682, https://doi.org/10.1023/A:1012534220165.
[59] Z.D. Xiang, J.S. Burnell-Gray, P.K. Datta, Conditions for codeposition of Al and Cr on Ni base superalloys by pack cementation process, Surf. Eng. 17 (2001) 287–294, https://doi.org/10.1179/026708401101517890.
[60] T.B. Massalski, H. (Hiroaki) Okamoto, ASM International, Binary Alloy Phase Diagrams, 2nd ed, ASM International, 1990.
[61] M.J. Bennett, A.T. Tuson, C.F. Knights, C.F. Ayres, Oxidation protection of alloy IN 738 LC by plasma assisted vapour deposited silica coating, Mater. Sci. Technol. (United Kingdom). 5 (1989) 841–852, https://doi.org/10.1179/mst.1989.5.8.841.
[62] F.J. Pérez, M.P. Hierro, F. Pedraza, M.C. Carpintero, C. Gómez, R. Tarín, Effect of fluidized bed CVD aluminide coatings on the cyclic oxidation of austenitic AISI 304 stainless steel, Surf. Coatings Technol. 145 (2001) 1–7, https://doi.org/10.1016/S0257-8972(01)01019-2.
[63] J. Stringer, Design of coatings for high temperature corrosion protection, in: R. Kossowsky, S.C. Singhal (Eds.), Surf. Eng., NATO ASI Series (Series E: Applied Sciences), vol 85, Springer, Dordrecht, 1984, pp. 561–587, , https://doi.org/10.1007/978-94-009-6216-3_37.
[64] T.D. Nguyen, J. Zhang, D.J. Young, Growth of Cr2O3 blades during alloy scaling in wet CO2 gas, Corros. Sci. 133 (2018) 432–442, https://doi.org/10.1016/j.corsci.2018.01.045.
[65] X. Zou, Y. Zhou, Z. Wang, S. Chen, B. Xiang, Y. Qiang, S. Zhu, Facile synthesis of α-Fe2O3 pyramid on reduced graphene oxide for supercapacitor and photo-degradation, J. Alloys Compd. 744 (2018) 412–420, https://doi.org/10.1016/j.jallcom.2018.02.126.
[66] K. Zhang, M.M. Liu, S.L. Liu, C. Sun, F.H. Wang, Hot corrosion behaviour of a cobalt-base super-alloy K40S with and without NiCrAlYSi coating, Corros. Sci. 53 (2011) 1990–1998, https://doi.org/10.1016/j.corsci.2011.02.022.